metals

MDPI

Article

Study on Pores in Ultrasonic-Assisted TIG Weld of Aluminum Alloy

Qihao Chen, Hongliang Ge, Chunli Yang *, Sanbao Lin and Chenglei Fan

State Key Laboratory of Advanced Welding and Joining, Harbin Institute of Technology, Harbin 150001, China; 14b909077@hit.edu.cn (Q.C.); ghl18714602893@163.com (H.G.); sblin@hit.edu.cn (S.L.); fclwh@hit.edu.cn (C.F.)
* Correspondence: yangcl9@hit.edu.cn; Tel: +86-451-8641-8775

Academic Editor: Houshang Alamdari
Received: 7 January 2017; Accepted: 8 February 2017; Published: 10 February 2017

Abstract: Ultrasonic-assisted tungsten inert gas welding was carried out on a thin plate of 2195 Al-Li alloy, and the characteristics of the weld pores were analyzed in terms of their size and porosity. The effects of welding speed and ultrasonic power on the porosity and size of the pores were investigated. The pores were found to occur primarily adjacent to the surface of the weld. The porosity decreased and the size increased with a decrease in welding speed. The effect of ultrasonic power on the characteristics of the pores was different from that of the welding speed. The porosity and size of the pores decreased and then increased with an increase in ultrasonic power. A relationship was found between the transient cavitation intensity and the characteristics of pores. An increasing transient cavitation intensity results in a decrease in the porosity and size of pores when the transient cavitation intensity is lower. However, it can result in an increase in the porosity and pore size when the transient cavitation intensity further increases. Finally, the influencing mechanism of cavitation on welding pores was discussed.

Keywords: aluminum alloy; ultrasonic power; TIG welding; pore; weld pool

1. Introduction

Aluminum-lithium alloy has been widely used in the aviation, aerospace, automobile and ship industries because of its excellent mechanical performance, high specific strength and corrosion resistance. Al-Li alloy can be joined with various welding methods, for example arc welding, friction stir welding, laser welding and electron beam welding. Solórzano et al. joined the 2091 Al-Li alloy with tungsten inert gas (TIG) welding and investigated the effect of TIG welding on the mechanical behavior of 2090 Al-Li alloy [1]. Chen joined 8090 Al-Li alloys with electron beam welding and studied the influence of welding parameters on the microstructures and mechanical properties of electron beam–welded 8090 Al-Li alloy plates [2]. Zhang et al. carried out a study on AA2060 Al-Li alloy using laser welding and Chen et al. joined 2A97 Al-Li alloy with friction stir welding [3,4].

TIG welding is widely used owing to its cost-effectiveness, ease of use and so on. However, some defects restrain the application of TIG-welded joints of Al-Li alloy. The most frequently occurring problem in TIG welding is porosity, which is the subject of this study. Some investigations on the pores in welding have been implemented. Yi et al. investigated the TIG dressing effects on weld pores and pore cracking of titanium weldments. The results showed that porosity redistribution by TIG dressing is due to fluid flow during the remelting of the weld pool and only weld pores less than 300 μm in size are redistributed or removed [5]. Leo et al. investigated the characteristics of pores in hybrid laser welding of an Al-Mg alloy. The results showed that the porosity area fraction increases with the laser power and the form of the micropores is related to the Mg vaporization [6]. Stützer et al. implemented a study on the pore formation in a super duplex stainless steel weld. The results suggested that the shielding gas, the filler metal and the welding speed have a great

influence on the pore formation [7]. Zhu et al. investigated the characteristics and formation mechanism of sidewall pores in narrow-gap gas metal arc welding of 5083 Al alloy. The results showed that the hydrogen is found to be the main cause of the pores. The pore amount and size increase along with the increasing welding current or the decreasing travel speed [8]. Huang et al. investigated the porosity in pulsed gas tungsten arc welding of aluminum alloys. The results indicated that the number of pores and the pores' area decrease significantly when the thickness of the welding root face is 2 mm [9].

Some of the reports on ultrasonic degassing in the casting field have been found so far and the results suggest that the ultrasound could decrease the number of pores for the casting [10,11]. The degassing effect is mainly related to the ultrasonic power and melt temperature [12]. Owing to the excellent effect of ultrasound on the microstructure in the casting field, many scholars have tried to apply ultrasound in the course of TIG welding. There are primarily three ways to implement ultrasound. In the first method, the ultrasound propagates into the weld pool from the arc space. Sun et al. directly imposed ultrasonic vibration on the welding arc by an ultrasonic horn; the vibration propagated into the weld pool through the arc space [13]. Qi et al. made the ultrasound propagate into the weld pool using a high-frequency pulse TIG process [14]. He et al. introduced an ultrasound to the weld pool using a high-frequency current to modulate the plasma arc [15,16]. The second route is the direct propagation of the ultrasound into the weld pool through the base material [17,18]. The third route is propagation of the ultrasound into the weld pool through the filler metal or ultrasonic probe. The ultrasound propagated into the weld pool using ultrasonically vibrating filler metal [19]. Yuan et al. introduced an ultrasonic vibration into the weld pool by dipping an ultrasonic probe in the weld pool. This study shows that the introduction of an ultrasound can result in significant changes in the weld microstructure [20].

Ultrasonic energy could affect the fluid flow and solidification of the weld pool when the ultrasonic energy is introduced into the weld pool during TIG welding. Most scholars pay attention to the effect of ultrasound on weld grain refinement and few reports on ultrasonic degassing in TIG welding have been found. As an environment-protecting and resource-economizing method, ultrasonic degassing is more attractive. Thus, investigation on ultrasonic degassing in TIG welding is important. In this paper, ultrasonic degassing technology in TIG welding is introduced and the weld pore behavior of Al-Li alloy was investigated for the ultrasonic-assisted TIG welding method. A new ultrasonic degassing theory is proposed, which will lay the foundation for the practical application of ultrasound-assisted TIG welding technology.

2. Materials and Methods

A 2195 Al-Li alloy sheet (2 mm thick) was used, with the base material composition shown in Table 1. No filler metal was used during welding, and the bead weld in the surface of the base material was conducted. The welding direction was perpendicular to the rolling direction of the base material.

Table 1. Chemical composition of the studied materials (wt. %).

Material	Li	Ag	Si	Fe	Cu	Mg	Zr	Al
2195	1.00	0.40	0.03	0.16	4.02	0.15	0.11	Bal

The ultrasonic welding system used in this study was designed and developed by our laboratory. A schematic of the experimental apparatus is shown in Figure 1. The ultrasound propagates into the weld pool from base material. The system can not only input the ultrasonic wave to the weld pool through the base material during continuous welding but also control the time of ultrasonic application. The ultrasonic frequency is 35 KHz. To meet the research needs, the rolling ultrasonic horn is used. The horn can roll on the surface of the base material, and a discontinuous ultrasound can be achieved by controlling the output of the ultrasonic waveform. The use of a rolling ultrasonic horn can avoid damage to the ultrasound system resulting from the vertical movement of cylinder.

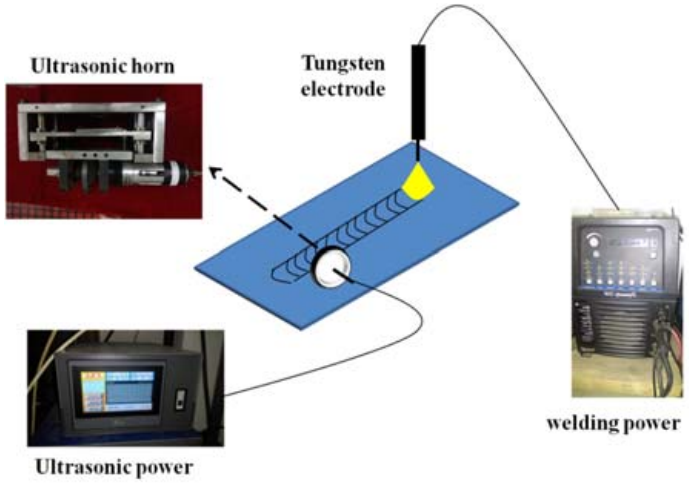

Figure 1. Schematic diagram of the ultrasonic-assisted TIG apparatus.

The surface of the base material is rigorously cleaned before welding to remove an oxide film and oil. Welding must be completed in a short time frame in order to avoid re-pollution. The welding current employs a variable-polarity square wave current. Shielding gas flow is 15 L/min, with an arc length of 3 mm. To ensure accuracy of the comparison, the front half of the weld is the original TIG weld, and the second half is the weld with discontinuous ultrasonic vibration. The working time and quitting time of the discontinuous ultrasounds are 0.5 s. To investigate the effect of welding speed and ultrasonic power on the pore behavior of the weld, the welding process parameters shown in Table 2 are used.

Table 2. Parameters in welding process parameters.

Specimens	Average Current I (A)	Duty Cycle δ (%)	Ultrasonic Power W (% × 800 W)	Welding Speed V (mm/min)
1	70	75	0	200
2	70	75	0	160
3	70	75	0	100
4	70	75	5	160
5	70	75	10	160
6	70	75	20	160
7	70	75	30	160
8	70	75	40	160

The weld longitudinal section A-A is analyzed and the schematic is shown in Figure 2.

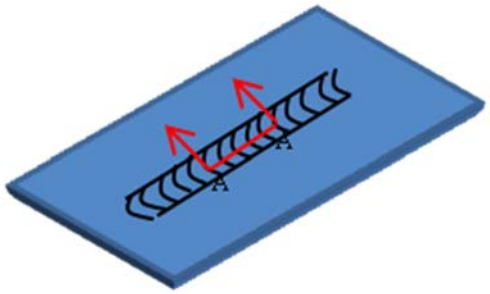

Figure 2. Schematic diagram of weld location for microstructure analysis.

Weld longitudinal sections are ground and mechanically polished. After that, the specimens are etched using Keller reagent (1 mL HF, 1.5 mL HCl, 2.5 mL HNO_3, and 95 mL H_2O). The microstructures for every welding condition are examined using the optical microscope (OM) (Keyence, Osaka, Japan). Several metallographic images of each parameter are analyzed using IPP software (Media Cybernetics, Rockville, MD, USA) to evaluate the porosity and size of the pores. The vibration of the weld pool is measured using a laser vibrometer (OFV-505/500) (Polytec, Karlsruhe, Germany). The result of the measurement is analyzed by fast Fourier transform using Matlab software (MathWorks, Natick, MA, USA).

3. Results and Discussion

3.1. Influence of Welding Speed on Pore Behaviors

In this section, the effect of the welding speed on the pore behavior is investigated. After welding, the longitudinal section of the weld center was used for porosity analysis. Figure 3 shows the weld microstructure resulting from different welding speeds. As shown in Figure 3, the pores were largely surface pores, and the number of pores was limited in the middle and bottom of the weld. This was a result of the thickness of the base material used for welding, which was thin, and generated bubbles could easily emerge from the weld pool. The bubbles would stay on the surface of the weld if they did not emerge from the weld pool completely.

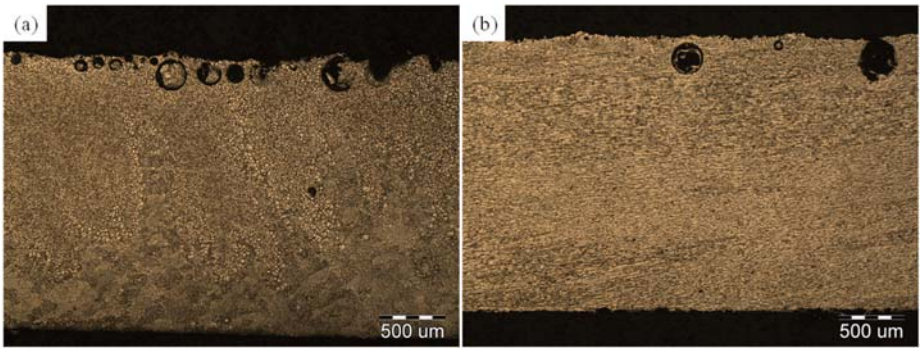

Figure 3. Pore distribution in longitudinal section of weld at different welding speeds: (**a**) 200 mm/min, (**b**) 100 mm/min.

Several metallographic pictures of each parameter were analyzed using the IPP software to examine the pore. In this paper, the porosity is defined as the total area of the pores contained in the unit length of the weld. The porosity and size of the pores with different welding speeds are shown in Figure 4. The porosity decreased significantly when the welding speed decreased. The porosity decreased by 13% when the welding speed decreased from 200 mm/min to 100 mm/min. In addition, the statistical results show that the maximum diameters of the pores in the weld were 87.57 μm, 115.78 μm, and 127.99 μm, when the welding speed decreased from 200 mm/min to 100 mm/min. Theoretically, it is not difficult to understand this result: the heat input increases as the welding speed decreases, and both the weld pool existence time and the grain growth time increase. The bubbles have more time to escape; therefore, the pore size increases and porosity decreases with the decreasing welding speed.

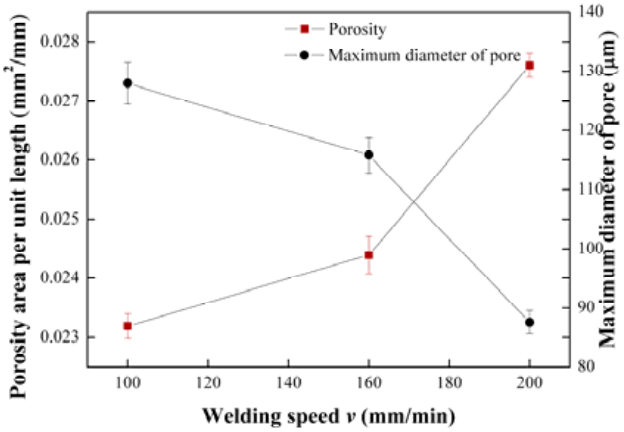

Figure 4. Porosity and pore size in longitudinal section of weld at different welding speeds.

3.2. *Influence of Ultrasonic Power on Pore Behaviors*

In Section 3.1, the influence of the welding speed on the porosity and pore size in the weld was obtained. In this section, the effect of ultrasonic power on pore behaviors is investigated. Figure 5 shows the weld metallographic picture with different ultrasonic powers. The porosity and pore size in the weld center with different parameters were analyzed using IPP software. The results are shown in Figure 6. Compared with the absence of ultrasound, the porosity in the weld significantly decreased when the ultrasonic treatment was implemented. The porosity was at its minimum and the porosity decreased by 39.19% when the ultrasonic power was 20%. The effect of changing the ultrasonic power on degassing was much greater than changing the welding speed. The porosity in the ultrasonic-assisted TIG weld significantly decreased compared with the absence of the ultrasound at the same welding speed. The porosity decreased with an increase in the ultrasonic power when the applied ultrasonic power was lower than 30%. However, the porosity increased when the ultrasonic power was higher than 30%. The variation of the pore size was very similar to the variation of the porosity in the weld. The pore size decreased with an increase in the ultrasonic power when the power was small. Still, the size increased when the ultrasonic power increased to a certain value.

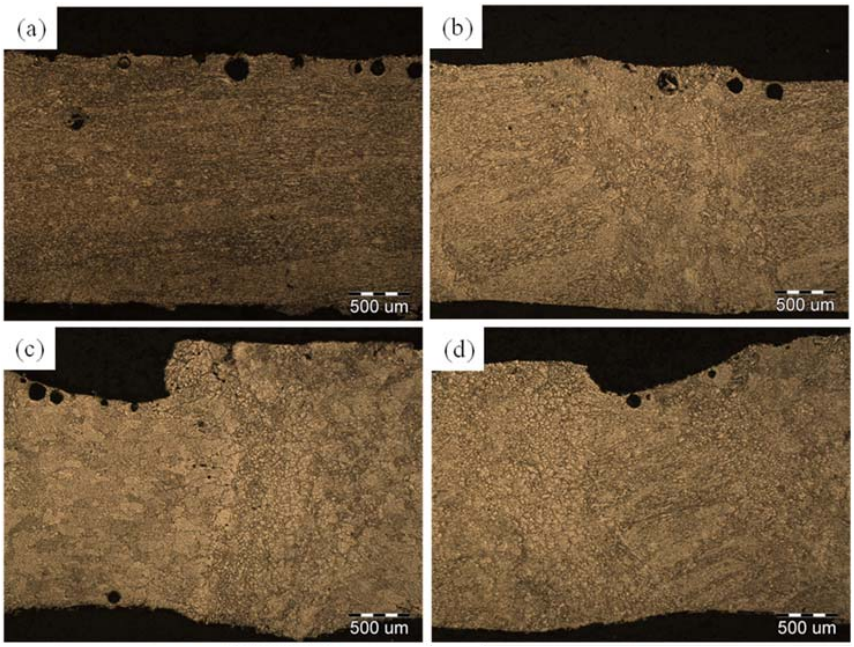

Figure 5. *Cont.*

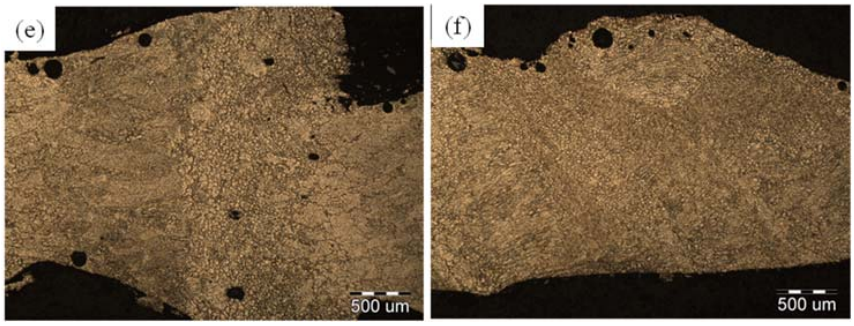

Figure 5. Pore distribution in longitudinal section of weld from different ultrasonic powers: (**a**) 0%, (**b**) 5%, (**c**) 10%, (**d**) 20%, (**e**) 30%, (**f**) 40%.

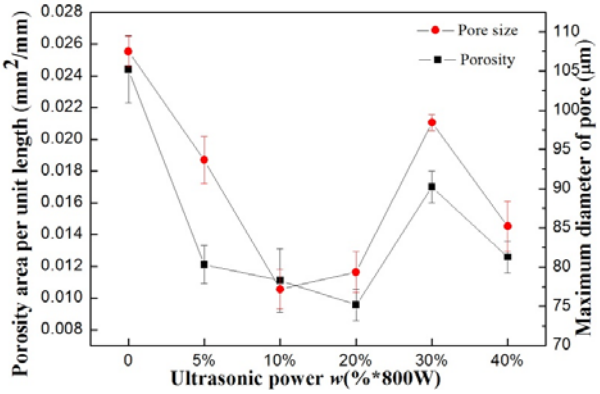

Figure 6. Porosity and pore size in longitudinal section of weld at different ultrasonic powers.

3.3. Analysis of Ultrasonic Behavior in Weld Pool

The ultrasound can result in non-linear cavitation in the melt when the ultrasonic power reaches a certain threshold value [21]. Cavitation can result in a large amount of harmonic waves, and the frequency is different from the applied ultrasonic frequency f_0 owing to the motion of the cavitation bubble. These harmonic waves are not random but have a regular distribution, which will produce two series of acoustics ($f_0/2$, $3f_0/2$, $5f_0/2$, ... and $2f_0$, $3f_0$, $4f_0$, ...) with the increase in cavitation. The characteristics of ultrasonic cavitation in the weld pool were analyzed to investigate the effect of ultrasound on the pore behavior.

The ultrasonic vibration on the surface of the weld pool was detected using a laser vibrometer. The weld pool size was small; thus, the overall difference between the vibration modes in different locations of the weld pool was not large. A single point measurement could instead be a multi-point measurement. The results in the time domain are shown in Figure 7 and the results in the frequency domain are shown in Figure 8. It was found that the relation between the ultrasonic cavitation intensity and the ultrasonic power is non-linear. For example, 5% power results in two secondary peaks of $f_0/2$ and $2f_0$; 10% and 20% power generate $3f_0$ and $4f_0$ peaks, and 40% power results in a $5f_0$ peak. However, the characteristics of 30% ultrasonic power do not meet this rule, and the cavitation strength is similar to 5% ultrasonic power. This result is similar to the relation between porosity and ultrasonic power. The cavitation intensity with 30% ultrasonic power and 5% ultrasonic power is similar, so the pore behavior is also similar.

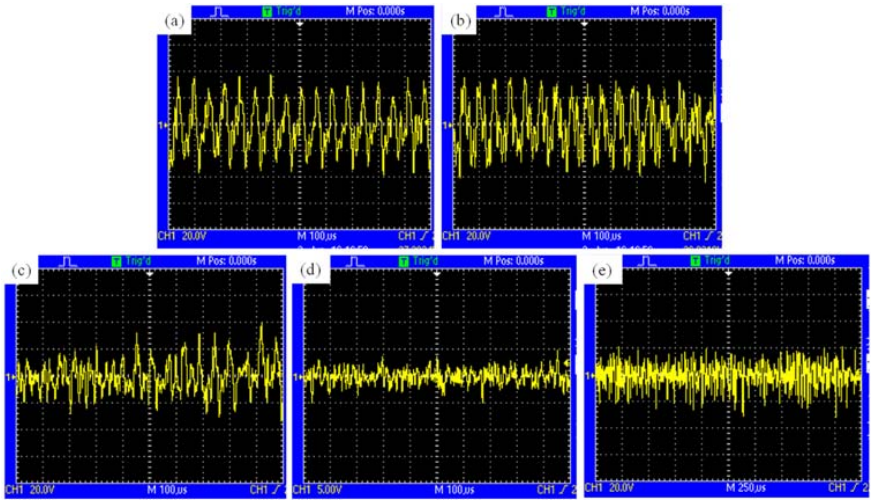

Figure 7. Vibration in time domain with different ultrasonic powers: (**a**) 5%, (**b**) 10%, (**c**) 20%, (**d**) 30%, (**e**) 40%.

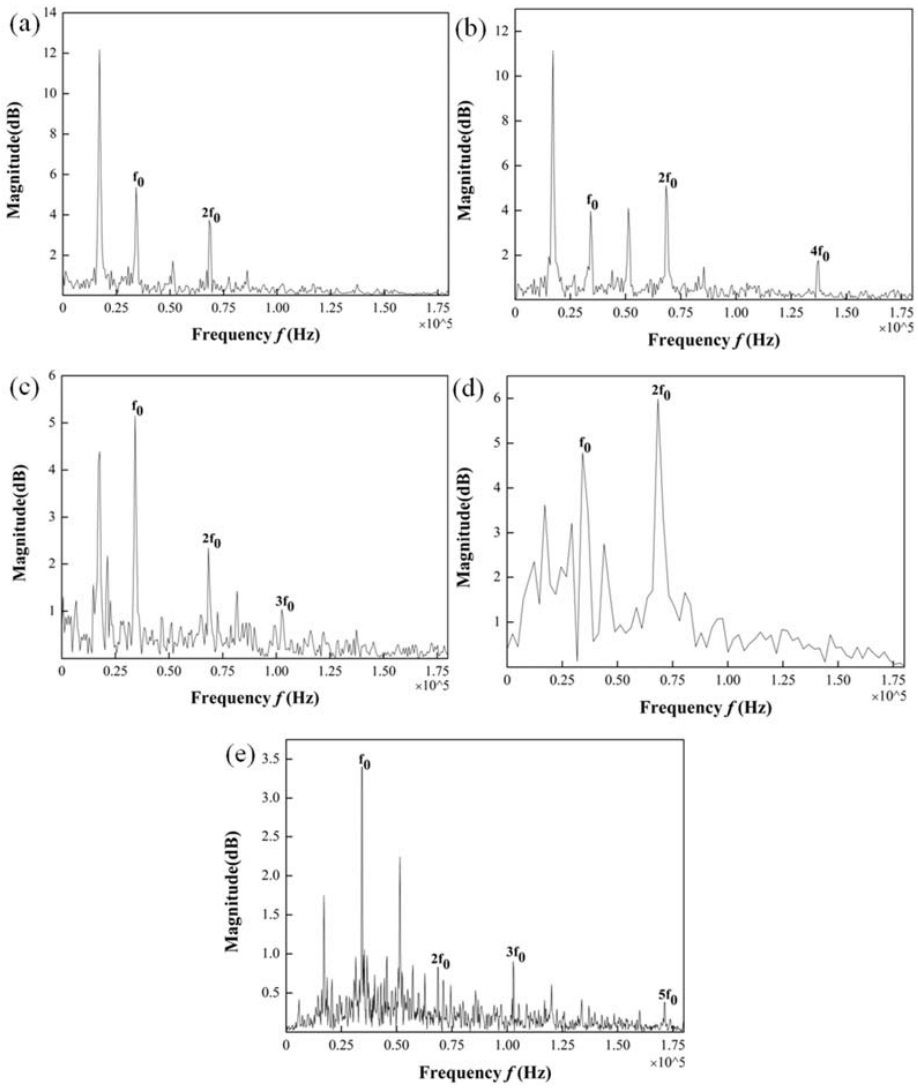

Figure 8. Vibration in frequency domain with different ultrasonic powers: (**a**) 5%, (**b**) 10%, (**c**) 20%, (**d**) 30%, (**e**) 40%.

Tzanakis et al. investigated the relation between the cavitation intensity and ultrasonic power, where the result also showed that the relation was non-linear [22]. The cavitation initiated more cavitation bubbles which oscillated non-linearly owing to the large-amplitude drivings. The cavitation bubbles dissipated mechanical energy by various processes, which should result in wave attenuation [23]. The energy attenuation decreased the acoustic pressure in the TIG weld pool, and. thus, the cavitation activity decreased.

3.4. Influence Mechanism of Ultrasonic Cavitation on Pore Behavior in the Weld Pool

Ultrasonic cavitation can be divided into steady and transient cavitation. As the ultrasonic cavitation intensity increases, the transient cavitation intensity gradually increases, while the proportion of steady cavitation gradually weakens. A large negative pressure in the bubble could promote free hydrogen into the bubble when the cavitation bubble expands [24]. The hydrogen is combined into H_2 and restrained in the bubble. The H_2 is excluded with the emersion of the bubble. The schematic is shown in Figure 9a.

Transient cavitation can also have a positive effect on the bubble, as shown in Figure 9b. The cavitation bubble can be broken by transient cavitation, which increases the number of bubbles. The gas migrates into the bubble and the probability of it escaping from the weld pool increases, thereby reducing the porosity of the weld. The transient cavitation decreases the bubble size, and the majority of bubbles can escape when the ultrasonic power is not large; thus, the porosity of the weld is decreased.

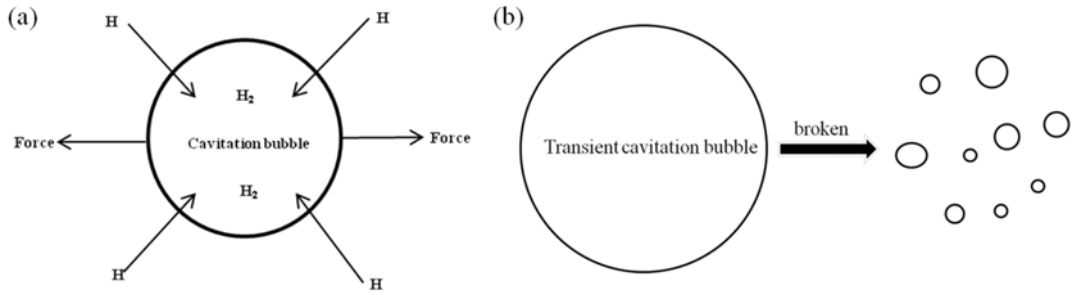

Figure 9. Effect of cavitation bubble on degassing by different routes: (**a**) cavitation bubble expands, (**b**) cavitation bubble collapses.

The transient cavitation intensity increased with an increase in the ultrasonic power and a larger transient cavitation intensity can result in a greater number of smaller bubbles. The minimal pore size that can emerge from the weld pool is described by Equation (1) [25].

$$v_e = \frac{2(\varrho_L - \varrho_G)gR^2}{9\eta} \quad (1)$$

where v_e is the velocity of emerging from the weld pool, ϱ_L and ϱ_G are the density of the melt and gas, respectively, g is the gravity constant, η is the viscosity of the melt and R the radius of the pore. The minimal pore size that can emerge from the weld pool is approximately 21 μm according to Equation (1). It is counteractive to degassing when the number of bubbles is higher than the required number and when the size of the bubbles is smaller than 21 μm. Eventually, the bubbles grow with each other, resulting in an increase in the bubble size and porosity, as shown in Figure 10.

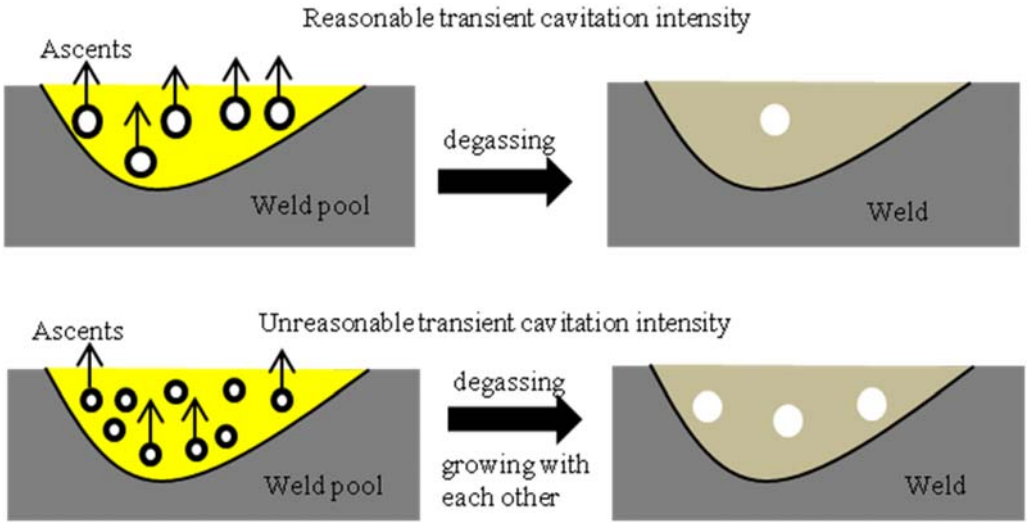

Figure 10. Effect of transient cavitation intensity on degassing in the weld pool.

4. Conclusions

(1) The welding speed can affect the porosity in the weld and the porosity decreases with a decrease in the welding speed. However, this effect is not significant. The porosity is only reduced by 13% when the welding speed decreases by 50%.

(2) The porosity and pore size of the weld with ultrasonic treatment is significantly decreased compared with the ordinary TIG weld. The porosity and pore size showed a tendency to decrease first and then increase with an increase in the ultrasonic power.

(3) There is an obvious influence of the transient cavitation intensity on the characteristics of pores in the weld. The micro-bubbles can escape easily when the transient cavitation is weaker. The volume and number of bubbles will increase when the transient cavitation intensity is greater than a certain degree.

Acknowledgments: This work was supported by the Key Program of the National Natural Science Foundation of China (Grant No. 51435004).

Author Contributions: Qihao Chen performed most of experiments and wrote this manuscript. Hongliang Ge analyzed the experimental data and gave some constructive suggestions. Chunli Yang, Sanbao Lin and Chenglei Fan participated in the discussion of the results and guided the writing of the article.

Conflicts of Interest: The authors declare no conflict of interest.

References

1. Solórzano, I.G.; Darwish, F.A.; de Macedo, M.C.; de Menezes, S.O. Effect of weld metal microstructure on the monotonic and cyclic mechanical behavior of tig welded 2091 Al-Li alloy joints. *Mater. Sci. Eng. A* **2002**, *348*, 251–261. [CrossRef]
2. Chen, S.C.; Huang, J.C. Influence of welding parameters on microstructures and mechanical properties of electron beam welded aluminium–lithium plates. *Mater. Sci. Technol.* **1999**, *15*, 965–978. [CrossRef]
3. Zhang, X.Y.; Huang, T.; Yang, W.X.; Xiao, R.S.; Liu, Z.; Li, L. Microstructure and mechanical properties of laser beam-welded AA2060 Al-Li alloy. *J. Mater. Process. Technol.* **2016**, *237*, 301–308. [CrossRef]
4. Chen, H.Y.; Fu, L.; Liang, P. Microstructure, texture and mechanical properties of friction stir welded butt joints of 2A97 Al Li alloy ultra-thin sheets. *J. Alloy. Compd.* **2017**, *692*, 155–169. [CrossRef]
5. Yi, H.J.; Lee, Y.J.; Lee, K.O. TIG dressing effects on weld pores and pore cracking of titanium weldments. *Metals* **2016**, *6*, 243. [CrossRef]
6. Leo, P.; Renna, G.; Casalino, G.; Olabi, A.G. Effect of power distribution on the weld quality during hybrid laser welding of an Al-Mg alloy. *Opt. Laser Technol.* **2015**, *73*, 118–126. [CrossRef]

7. Stützer, J.; Zinke, M.; Jüttner, S. Studies on the pore formation in super duplex stainless steel welds. *Weld. Word* **2017**, *61*, 351–359. [CrossRef]
8. Zhu, C.; Tang, X.; He, Y.; Lu, F.; Cui, H. Characteristics and formation mechanism of sidewall pores in NG-GMAW of 5083 Al-alloy. *J. Mater. Process. Technol.* **2016**, *238*, 274–283. [CrossRef]
9. Huang, Y.; Wu, D.; Lv, N.; Chen, H.; Chen, S. Investigation of porosity in pulsed GTAW of aluminum alloys based on spectral and X-ray image analyses. *J. Mater. Process. Technol.* **2016**, *243*, 365–373. [CrossRef]
10. Abramov, V.; Bulgakov, V.; Sommer, F. Solidification of aluminum alloys under ultrasonic irradiation using water-cooled resonator. *Mater. Lett.* **1998**, *42*, 27–34. [CrossRef]
11. Xu, H.; Han, Q.; Meek, T.T. Effect of ultrasonic vibration on degassing of aluminum alloys. *Mater. Sci. Eng. A* **2008**, *473*, 96–104. [CrossRef]
12. Puga, H.; Barbosa, J.; Seabra, E.; Ribeiro, S.; Prokic, M. The influence of processing parameters on the ultrasonic degassing of molten AlSi9Cu3 aluminium alloy. *Mater. Lett.* **2009**, *63*, 806–808. [CrossRef]
13. Sun, Q.J.; Lin, S.B.; Yang, C.L.; Fan, Y.Y.; Zhao, G.Q. The arc characteristic of ultrasonic assisted TIG welding. *China Weld.* **2008**, *17*, 52–57.
14. Qi, B.J.; Yang, M.X.; Cong, B.Q.; Liu, F.J. The effect of arc behavior on weld geometry by high-frequency pulse GTAW process with 0Cr18Ni9Ti stainless steel. *Int. J. Adv. Manuf. Technol.* **2013**, *66*, 1545–1553. [CrossRef]
15. He, L.B.; Yang, P.; Li, L.M.; Wu, M.S. The ultrasonic characteristics of high frequency modulated arc and its application in material processing. *Ultrasonics* **2014**, *54*, 2178–2183. [CrossRef] [PubMed]
16. He, L.B.; Wu, M.S.; Li, L.M.; Hao, H.W. Ultrasonic generation by exciting electric arc: A tool for grain refinement in welding process. *Appl. Phys. Lett.* **2006**, *89*, 131504–131505. [CrossRef]
17. Cui, Y.; Xu, C.L.; Han, Q.Y. Microstructure Improvement in Weld Metal Using Ultrasonic Vibrations. *Adv. Eng. Mater.* **2006**, *9*, 161–163. [CrossRef]
18. Dai, W.L. Effects of high-intensity ultrasonic-wave emission on the weldability of aluminum alloy 7075-T6. *Mater. Lett.* **2003**, *57*, 2447–2454. [CrossRef]
19. Watanabe, T.; Shiroki, M.; Yanagisawa, A.; Sasaki, T. Improvement of mechanical properties of ferritic stainless steel weld metal by ultrasonic vibration. *J. Mater. Process. Technol.* **2010**, *210*, 1646–1651. [CrossRef]
20. Yuan, T.; Kou, S.; Luo, Z. Grain refining by ultrasonic stirring of the weld pool. *Acta Mater.* **2016**, *106*, 144–154. [CrossRef]
21. Matsunaga, T.; Ogata, K.; Hatayama, T. Effect of acoustic cavitation on ease of infiltration of molten aluminum alloys into carbon fiber bundles using ultrasonic infiltration method. *Compos. Part A Appl. Sci. Manuf.* **2007**, *38*, 771–778. [CrossRef]
22. Tzanakis, I.; Lebon, G.S.B.; Eskin, D.G.; Pericleous, K.A. Characterisation of the ultrasonic acoustic spectrum and pressurefield in aluminium melt with an advanced cavitometer. *J. Mater. Process. Technol.* **2016**, *229*, 582–586. [CrossRef]
23. Louisnard, O. A simple model of ultrasound propagation in a cavitating liquid. Part I: Theory, nonlinear attenuation and traveling wave generation. *Ultrason. Sonochem.* **2012**, *19*, 56–65. [CrossRef] [PubMed]
24. Naji Meidani, A.R.; Hasan, M. A study of hydrogen bubble growth during ultrasonic degassing of Al-Cu alloy melts. *J. Mater. Process. Technol.* **2014**, *147*, 311–320. [CrossRef]
25. Li, J.W.; Momono, T.; Tayu, Y.; Fu, Y. Application of ultrasonic treating to degassing of metal ingots. *Mater. Lett.* **2008**, *62*, 4152–4154. [CrossRef]